



Investigating 2D WS₂ supercapacitor electrode performance by Kelvin Probe Force Microscopy

Journal:	<i>Journal of Materials Chemistry A</i>
Manuscript ID	TA-ART-03-2020-003383.R1
Article Type:	Paper
Date Submitted by the Author:	22-May-2020
Complete List of Authors:	<p>Sambath Kumar, Kowsik; Univeristy of Central Florida, NanoScience Technology Center; UNIVERSITY OF CENTRAL FLORIDA</p> <p>Choudhary, Nitin; University of Central Florida, NanoScience Technology Center</p> <p>Pandey, Deepak; University of Central Florida</p> <p>Ding, Yi; University of Central Florida, NanoScience Technology Center</p> <p>Hurtado, Luis; University of Central Florida, Materials Science & Engineering</p> <p>Chung, Hee-Suk; Korea Basic Science Institute,</p> <p>Tetard, Laurene; University of Central Florida, NanoScience Technology Center</p> <p>Jung , Yeonwoong; University of Central Florida, Materials Science & Engineering</p> <p>Thomas, Jayan; University of Central Florida, NanoScience Technology Center; CREOL, College of Optics and Photonics</p>

ARTICLE

Investigating 2D WS₂ supercapacitor electrode performance by Kelvin Probe Force Microscopy

Kowsik Sambath Kumar^{a,b}, Nitin Choudhary^b, Deepak Pandey^{a,b}, Yi Ding^{a,b}, Luis Hurtado^b, Hee-Suk Chung^c, Laurene Tetard^{b,d}, Yeonwoong Jung^{a,b,e} and Jayan Thomas^{*a,b,f}

Electrode materials used in energy storage devices undergo structural and chemical changes during cycling, which impact the long-term stability of the device. However, the phenomena behind how these changes occur at electrode surfaces remain unclear. Here we investigate the evolution of two-dimensional (2D) supercapacitor electrodes during cycling via a multifaceted approach. We propose a novel method to monitor the strain caused by cycling the 2D tungsten disulfide (WS₂)-based electrode by mapping the work function of the electrode at different electrochemical cycling intervals using Kelvin Probe Force Microscopy (KPFM). To support our study, the evolution of the 2D WS₂-based electrode over the course of repeated cycling is evaluated using Raman spectroscopy. The results reveal that during cycling, a strain is developed in the WS₂ layers due to the intercalation/deintercalation of the electrolyte ions. As a result, the available electrochemical active sites increases leading to an increase in capacitance. This new approach enables to understand the evolution of electrodes with cycle life and is expected to benefit the development of more efficient and long-lasting energy storage devices.

Received 00th January 20xx,
Accepted 00th January 20xx

DOI: 10.1039/x0xx00000x

1 Introduction

The energy industry is unceasingly looking for a complete transition from the exhaustive use of fossil fuels to renewable energy resources in the hope of meeting the ever-increasing energy demands of the consumer industry such as electric vehicles, e-paper, cordless tools, and grid storage, just to name a few.^{1, 2} While this paradigm shift towards the renewable energy is underway, the next biggest challenge in setting up new energy economies would be the development of efficient energy storage systems/devices. An ideal efficient energy storage system is expected to deliver energy for a longer period (hundreds of thousands of cycles) without compromising its efficiency. Energy storage devices with a longer cycle life would help in avoiding frequent replacement of devices, cut costs of replacement, and recycling the dead batteries or supercapacitors. Thus, cycle life is becoming an increasingly important parameter to be focused on developing efficient energy storage devices. Currently, supercapacitor is one of the best energy storage devices for applications requiring long cycle life. On the contrary to batteries with bulk charge storage, supercapacitors store charges on the surface, which enable them to run for hundreds of thousands of cycles without causing considerable structural damage. Several research efforts are focussed on developing long-lasting electrode materials. These efforts involve developing nanostructured or hybrid electrode materials for enhancing the

surface area, conductivity, capacitance, and cycle life, etc. Most of these studies do not analyze the structural or chemical changes happening at the nano level of the electrode surface in depth. These changes are responsible for the inferior or superior performance of the electrodes. As mentioned earlier, the cycle life of the supercapacitor electrode has an economic and environmental impact. Therefore, it is necessary to develop a qualitative analysis for investigating the basic mechanism responsible for the structural or chemical changes occurring in the electrodes during cycling. For instance, a number of studies investigating the cycling performance of the supercapacitor electrodes infer that wetting of the electrode surface plays a critical role in the increase of capacitance during cycling.⁴⁻⁸ A direct proof of this inference has not yet been reported. Uncovering the underlying mechanisms responsible for such a change in electrode performance during cycling is critical to design better-performing electrodes. Qualitative analysis techniques should be developed for exploring the chemical or structural changes of the electrode materials during cycling. Kelvin probe force microscopy (KPFM) is one such tool that facilitates nanometer-scale imaging of the surface potential on a wide range of materials. KPFM aids in measuring the local contact potential difference between a conducting atomic force microscopy (AFM) tip and the sample. Using the local contact potential difference value, the surface potential or work function of the electrode material can be mapped with high spatial resolution.⁹ A relationship between the work function change and the surface-level changes caused in the electrode structure during cycling gives vital information towards engineering electrodes at nano level.¹⁰

Also, developing new materials and rational engineering of their nanostructures are essential to achieve high surface areas, exposure of more electroactive sites, fast kinetics of ion and electron transport and high cycle life.^{8, 11} 2D nanomaterials are one of the best candidates among nanostructured materials for supercapacitors as they are single to few atomic layers thick, providing enhanced surface area and high mechanical integrity.¹² Among the 2D nanomaterials, transition metal dichalcogenides (TMDs) such as

^a Department of Materials Science and Engineering, University of Central Florida, Orlando, Florida 32816, United States

^b NanoScience Technology Center, University of Central Florida, Orlando, Florida 32816, United States

^c Analytical Research Division, Korea Basic Science Institute, Jeonju 54907, South Korea

^d Department of Physics, University of Central Florida, Orlando, Florida 32816, United States

^e Department of Electrical and Computer Engineering, University of Central Florida, Orlando, Florida 32816, United States

^f CREOL, College of Optics and Photonics, University of Central Florida, Orlando, Florida 32816, United States.

tungsten disulfide (WS_2), molybdenum disulfide (MoS_2) or molybdenum diselenide ($MoSe_2$) have attracted significant attention as capacitive materials owing to their intrinsically layered structure and high surface area, which favors fast ionic adsorption and transport through them.¹³⁻¹⁶ Among the TMDs, WS_2 has attracted huge attention in energy storage due to their 2D covalently bonded S-W-S layers providing huge surface area. The W atoms have a wide range of oxidation states varying from +2 to +6, suggesting WS_2 to be a promising pseudocapacitive material for energy storage applications.¹⁷ In a previous work, Thomas et al. developed a highly single-crystalline tungsten trioxide (WO_3) core and WS_2 shell electrode on tungsten foil following a spontaneous oxidation/sulfurization method.¹⁸ This hybrid 2D nanomaterial offers seamless interfaces and excellent electrochemical stability with unprecedented cycle life.

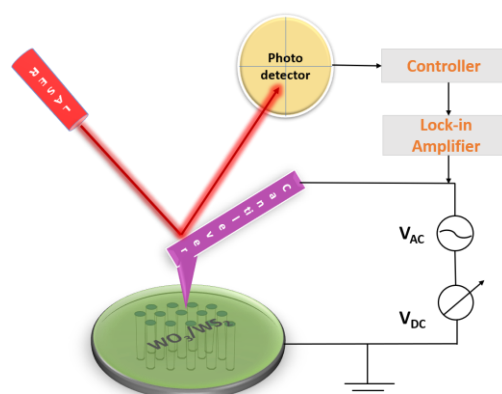
In our work we synthesized WS_2 electrode via chemical vapor deposition (CVD) and investigated their electrochemical performance at different electrochemical cycles. We probe the local variations in work function in the WS_2 electrode using KPFM and compare them to the change in capacitance of the electrode at different cycles. We discovered that underlying mechanism responsible for the change in capacitance was attributed to the strain effect on the interlayer spacing of the electrode materials. This strain led to an increase in the redox behavior of the electrodes during cycling, which was further studied by estimating the capacitance contribution from different charge storage mechanisms. We also evaluated the effect of cycling on the 2D material lattice using Raman spectroscopy and backed our findings from KPFM.

2 Experimental Methods

2.1 Preparation of WS_2 electrode

Tungsten (W) foil was sequentially cleaned by ultrasonication in acetone, hydrochloric acid, ethanol, and DI water. The preparation of the WS_2 electrode involved two steps. In the first step, a vertically aligned array of WO_3 nanowires were prepared on the tungsten foil

and the furnace was maintained at 850 °C for 40 minutes followed by natural cooling.¹⁸



Scheme. 1 Schematic of KPFM with their components

2.2 Characterization of the electrodes

The microstructure and morphology of the electrode were examined by scanning electron microscopy (SEM; ZEISS Ultra-55) and transmission electron microscopy (TEM; JEOL ARM200F Cs-corrected). The composition and structure of the materials were investigated by Raman spectroscopy (WITec 300 RA confocal system with 532 nm laser excitation). The surface topography and the surface potential of the electrode materials were studied by atomic force microscopy (AFM) and KPFM (NanoIR2 AFM Bruker using PR-EX-KPFM cantilevers). The sample preparation for the AFM and KPFM involved collecting the WS_2 electrode after each stage of cycling (pristine, 2500 and 10000 cycles) and rinsing it with DI water to remove the loosely attached electrolyte before they are

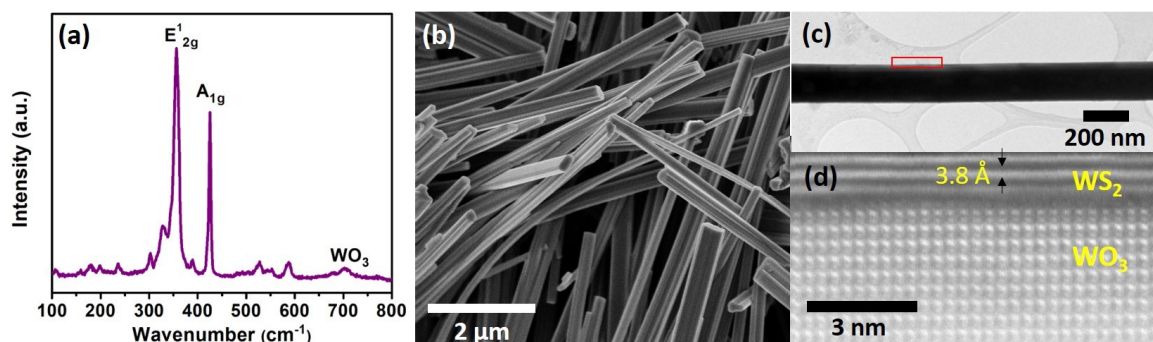


Fig. 1 (a) Raman spectra of the WS_2 electrode. (b) SEM image of WS_2 electrode. (c) Low-magnification bright field TEM image of a WS_2 electrode. (d) HAADF-STEM image of the WS_2 electrode in the portion marked in the red box in (c).

by drop-casting 10 wt% potassium hydroxide (KOH) solution followed by spin coating. Then the tungsten foil was further heated at 650 °C in a thermal furnace for 2 hours followed by rinsing in deionized (DI) water and drying at room temperature. In the second step, the tungsten foil was sulfurized in a CVD system by keeping pure sulfur (S) source along with the tungsten foil with nanowires in a quartz tube furnace. Argon gas was flushed through the furnace,

characterized by AFM and KPFM. The sample film was carefully removed from the W foil and was mounted on a 12 mm metallic disc using conductive silver paint used to ground the sample with respect to the tip. The schematic of KPFM measurements with their components is shown in Scheme. 1. KPFM measurements were performed using a two-pass method. During the first pass, the

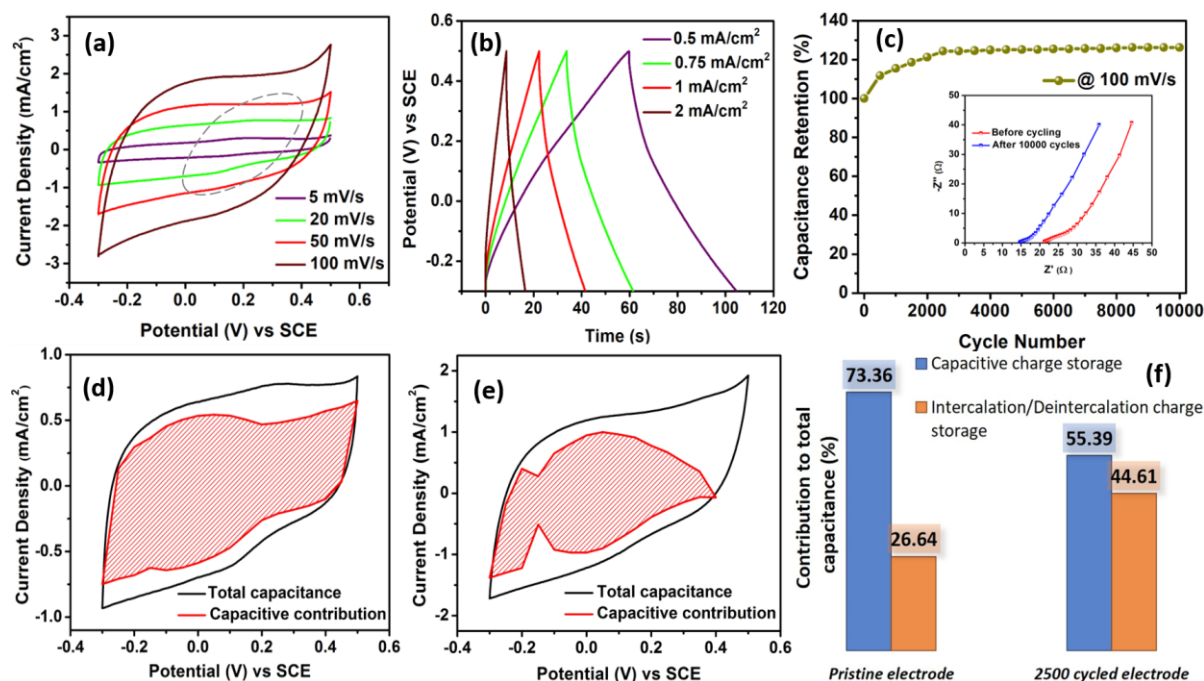


Fig. 2 (a) CV curves of WS_2 electrode at different scan rates. Dotted region shows the distorted part of CV curves (b) GCD curves of WS_2 electrode at different current densities. (c) Capacitance retention at different cycle numbers for the WS_2 electrode. Inset in (c) shows the Nyquist plots for the WS_2 electrode before and after cycling. (d-f) Calculation of capacitance contribution arising from the capacitive charge storage (shaded region) and intercalation/deintercalation charge storage mechanisms at a scan rate of 20 mV s^{-1} for (d) pristine WS_2 electrode and (e) 2500 cycled WS_2 electrode. (f) Capacitance contribution (%) plot for pristine WS_2 electrode and that after 2500 cycles.

cantilever was mechanically driven at its resonant frequency to determine the topography of the sample. During the second-pass scan, the cantilever was lifted by a fixed distance (30 nm) to minimize the effect of short-range van der Waals forces and maximize the effect of long-range forces. A bias was applied to the cantilever, which includes a DC and an AC component, to obtain a potential difference $\Delta V = V_{\text{DC}} + V_{\text{AC}}$ between the tip and the sample. The AC component was used to electrically vibrate the cantilever at its resonant frequency while V_{DC} was adjusted by the AFM controller to null the force gradient resulting from the differences between the tip work function (ϕ_{tip}) and the sample work function (ϕ_s). $V_{\text{DC}} = V_{\text{CPD}}$ is recorded and used to obtain the KPFM maps. The work function of the sample ϕ_s is determined using the relationship $\phi_s = \phi_{\text{tip}} - e V_{\text{CPD}}$, where ϕ_{tip} is constant for a given tip (i.e. 5.16 eV), e is the electronic charge and V_{CPD} is contact potential difference between tip and the sample (WS_2).

Each of the KPFM probe was calibrated to determine ϕ_{tip} . The calibration process involves the KPFM measurement of a freshly-exfoliated HOPG flake and evaluating the work function of HOPG using $\phi_{\text{HOPG}} = \phi_{\text{tip}} - e V_{\text{CPD}}$, where ϕ_{HOPG} (4.6 +/- 0.1 eV). The V_{CPD} was extracted by averaging the values of the KPFM map on raw datasets. For each kind of supercapacitor sample (before and after cycling), at least 3 sets of samples were characterized. On each sample, at least 3 positions were selected to confirm the repeatability of the measurements.

Electrochemical measurements, including cyclic voltammetry (CV), electrochemical impedance spectroscopy (EIS), and

galvanostatic charge/discharge (GCD) measurements were performed using an electrochemical workstation (SP-150, Bio-Logic, USA). The electrochemical characterization of WO_3/WS_2 core/shell nanowires on W foil with an area of 1 cm^2 were performed in a three-electrode cell set-up by using 0.1 M sodium sulfate (Na_2SO_4) electrolyte. Platinum (Pt) foil and saturated calomel electrode (SCE) were used as counter electrode and the reference electrode, respectively.

3 Results and Discussions

Fig. 1a represents the Raman spectrum of the electrode revealing the presence of WS_2 . The presence of two strong bands at 356 cm^{-1} and 421 cm^{-1} correspond to the in-plane E_{2g} and out-of-plane A_{1g} phonon mode, respectively.¹⁹ The presence of WO_3 core is evident from the band appearing at 701 cm^{-1} which corresponds to O-W-O bond stretching.²⁰ SEM and TEM reveal the microstructure and morphology of the as prepared WO_3/WS_2 nanowires. As seen in the SEM image of the WO_3/WS_2 nanowires (Fig. 1b), the electrode exhibits a very dense growth of the nanowires of $\sim 8 - 10 \mu\text{m}$ in length and $\sim 150 - 200 \text{ nm}$ in diameter, with an aspect ratio of ~ 50 . Such one-dimensional nanostructures provide a large surface area for charge storage as well as short diffusion paths for ion transport. The bright-field TEM image (Fig. 1c) shows a uniform diameter of a single nanowire throughout its length. The high-angle annular dark field scanning TEM (HAADF-STEM) image of the nanowire (Fig. 1d) depicts that the WO_3 core is uniformly covered with well-spaced 2D WS_2

layers. We can evidently see the atomically sharp interface in the core/shell WO_3/WS_2 nanowire.

The electrochemical performance of the WS_2 electrode was evaluated in 0.1 M Na_2SO_4 electrolyte in the potential range of -0.3 to 0.5 V vs SCE. The electrode exhibited a dominant EDLC behaviour with nearly symmetrical curves and delivered high areal capacitance of 51 mF cm^{-2} at 5 mV s^{-1} . Though the electrode exhibited EDLC behaviour, a slightly distorted CV curves with small peaks could be noticed (Fig. 2a), indicating that some redox reactions take place due to the intercalation of sodium ions into the 2D WS_2 layers. The dotted region in Fig. 2a indicates the peaks seen at lower scan rates such as 5 and 20 mV s^{-1} caused by the redox reaction and it almost diminishes away when the scan rate is increased. Typically, at low scan rates, redox reactions compared to capacitive reactions have larger contribution to charge storage than at higher scan rates. This happens because at lower scan rates, electrolyte ions get enough time to intercalate/deintercalate into WS_2 layers. The redox reactions caused by the Na^+ ion intercalation can be given by the equation $\text{WS}_2 + \text{Na}^+ + \text{e}^- = \text{WS-Na}^+$.²¹ As seen in Fig. 2b, the GCD curves exhibited nearly linear and symmetrical curves at different current densities and correlated well with the CV curves for the charge storage. The core WO_3 provides robustness for the electrodes for long term stability of the electrodes. At the surface of the nanowires, as more and more WS_2 layers are opened due to the intercalation-deintercalation of Na^+ ion with cycling, more electrochemically active sites are available for electrochemical energy storage. This was evident from the increase in the electrode capacitance during cycling up to 2500 cycles as shown in Fig. 2c. Because of this intercalation-deintercalation, a permanent strain accumulates into the lattice of WS_2 ,^{22, 23} which keeps on increasing for nearly 2500 cycles and relaxes thereafter, as seen in Fig. 2c. During cycling, the WS_2 layers experience the maximum strain at 2500 cycles, after which it can easily accommodate more Na^+ ions. That is the point at which the electrode gets stabilized and maintains its capacitance up to 10000 cycles with an unprecedented 100% capacitance retention. This strain also causes the resistance of the electrode to decrease as more active sites are available for storing electrolyte ions over cycling, as shown in the inset of Fig. 2c.³ The EIS acquired before and after cycling exhibited a drastic decrease in the ESR and charge transfer resistance of the electrode. To estimate the individual capacitance contribution arising from the EDLC/capacitive and redox/intercalation-deintercalation charge storage mechanism, we have used the 20 mV s^{-1} CV recorded for pristine WS_2 electrode. The details of estimating the capacitance contributions due to capacitive and intercalation/deintercalation charge storage mechanisms from CV curves is given in Supporting Information. The shaded region in Fig. 2d shows that the capacitive charge storage mechanism is dominant over the redox mechanism for a pristine WS_2 electrode. The strain causing the increase in the interlayer spacing is supposed to enhance the redox contributed charge storage after 2500 cycles as more Na^+ ions can be intercalated

into the WS_2 layers. So, the CV profile of the WS_2 electrode was again recorded at 20 mV s^{-1} after 2500 cycles of charge-discharge. The shaded region in Fig. 2e denoting capacitive charge storage has considerably decreased in this case, that the contribution from the redox mechanism has increased. This clearly shows that the increased interlayer spacing of the electrodes does play a role in enhancing the charge storage. The capacitance contribution plot is shown in Fig. 2f shows the capacitive contribution of the WS_2 electrode decreasing from 73.36% to 55.39%, while the redox contribution of the electrode increasing from 26.64% to 44.61%. This enhancement of the redox mechanism is a result of the interlayer spacing increase in the WS_2 layers caused over the period of 2500 cycles due to the constant intercalation and deintercalation of Na^+ ions. To further determine the potential origin of this behaviour, we collected WS_2 from the electrodes at different stages of cycling and mapped their surface potential using KPFM, which is directly related to the work function of the material (Fig. 3). A conductive AFM tip was used to estimate the contact potential difference (V_{CPD} , see methods) between the tip and WS_2 , which is proportional to the difference between the work function of the tip and the work function of the sample. The measurements were performed on the pristine electrode before cycling, after 2500 cycles, and after 10000 cycles.

AFM topographical images of the WS_2 electrode before cycling (Fig. 3a), after 2500 cycles (Fig. 3d), and after 10000 cycles (Fig. 3g) indicate slight changes in grain sizes although the arrangement remained dense at all stages. VCPD values captured by KPFM before cycling (Fig. 3b), after 2500 (Fig. 3e), and after 10000 cycles (Fig. 3h) reveal significant changes in the estimated work function of the material. The variation can be attributed to the strain induced in the WS_2 lattice as a result of intercalation and deintercalation of Na^+ ions during the continuous charge/discharge cycles. It is well-studied that the intercalation of hetero-atoms into the layered structure of WS_2 causes the development of strain in the lattice.^{22, 23} When the strain is induced in the interior domains of WS_2 , the Fermi velocity $\mathbf{vF} = \left[\frac{\partial E_{\vec{k}}}{\hbar \partial \vec{k}} \right] d\mathbf{E}_{\vec{k}} = \mathbf{E}_F$ depending upon the wave vector \mathbf{k} decreases with the increasing strain, leading to an increase in the work function.²⁴ This dependency of work function on the strain induced in WS_2 lattice has also been investigated by Meng et. al²⁵ using density functional theory (DFT) to find the correlation between the applied strain, generated band gap, and modified work function of WS_2 . The results suggest that with applied strain, the work function tends to increase due to the change in lattice parameter and the interatomic distances, which leads to modulation of hybridization energy of 3p orbitals of S atoms and 4d orbitals of W atoms.²⁶ The KPFM data shows that before cycling, the average work function of WS_2 was ~ 4.82 eV (Fig. 3c), which increased as the electrode underwent the initial cycling. This is accompanied by a strain in WS_2 due to intercalation/deintercalation of Na^+ ions, also evidenced by the shift of the out-of-plane phonon A_{1g} mode from 424 to 424.5

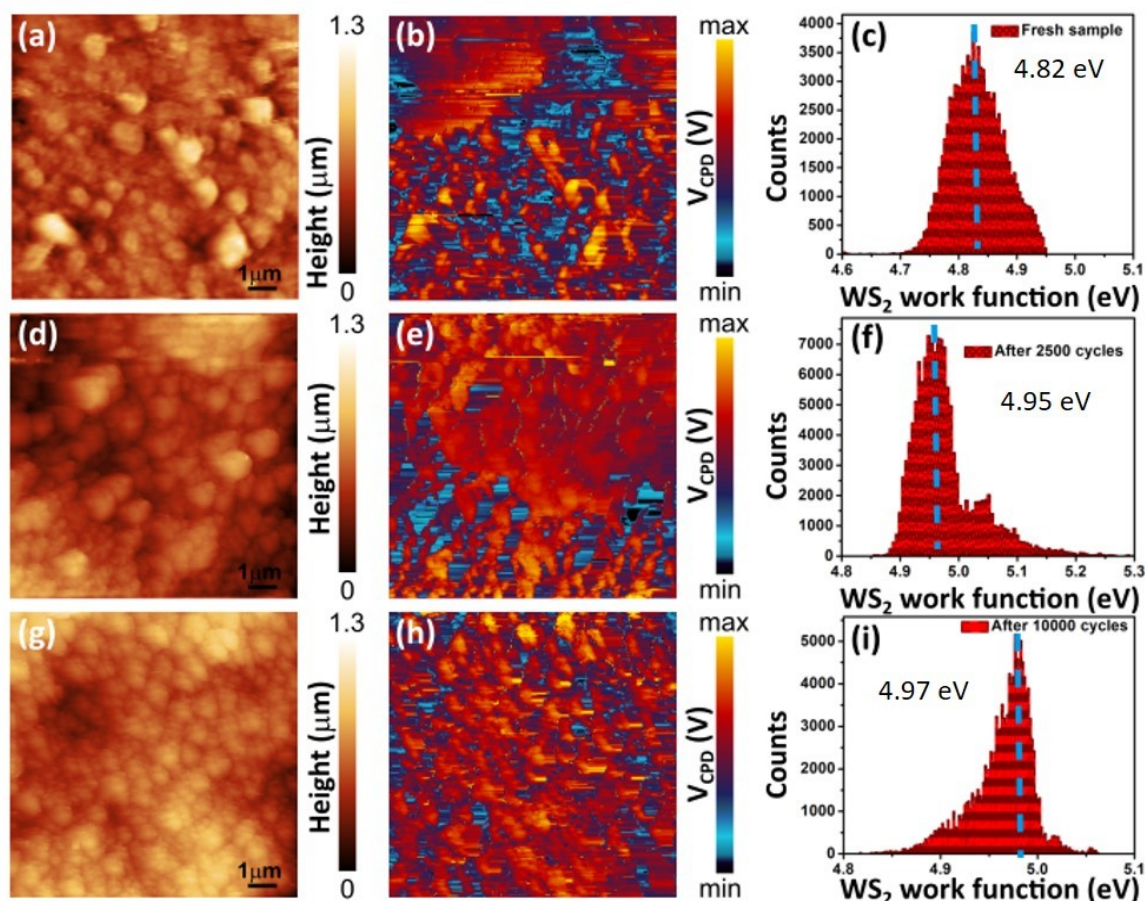


Fig. 3 (a,d,g) AFM topographical images of the WS₂ electrode at the initial, 2500th, and 10000th cycles. (b,e,h) KPFM signal images of the WS₂ electrode at the initial, 2500th, and 10000th cycles showing the relative V_{CPD} measured across the electrode. (c, f, i) Work function histogram of the WS₂ electrode calculated from the KPFM images captured at the initial, 2500th, and 10000th cycles.

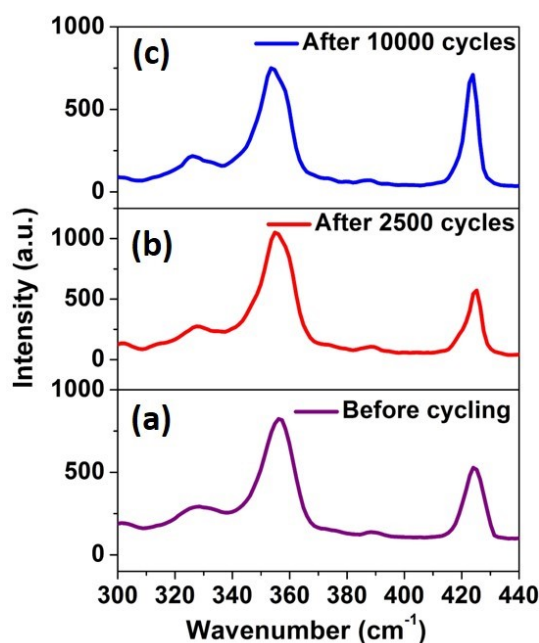


Fig. 4 Raman spectra of the electrodes (a) as-synthesized, (b) after 2500 cycles and (c) after 10000 cycles.

cm^{-1} in the Raman spectrum acquired after 2500 cycles and the decrease in the width of the band (Fig. 4b). As the interlayer spacing between the WS₂ layers expands to accommodate the sodium ions, the increased access for the electrolyte ions (Na^+) to the electrochemically active sites leads to an increase in the capacitance. In our electrode, this phenomenon displayed an increase to 125% of the initial capacitance, which reached a maximum after 2500 cycles, as shown in Fig. 2c. The increased strain results in an increase in work function to ~ 4.95 eV (Fig. 3f) and a softening of the out-of-plane phonon mode. After 2500 cycles, no further strain effect could be observed on the WS₂ lattice. Subsequently, the available electrochemical surface area remained constant and no significant variation in the capacitance was observed. A very small change in the work function of the WS₂ electrode to ~ 4.97 eV observed after 10000 cycles (Fig. 3i) was also accompanied by a slight shift in the E_{1-2g} and A_{1g} of the electrode indicating infinitesimal strain (Fig. 4c). As the electrode's interlayer spacing has reached its limit of accommodating strain, the capacitance also remained stable after 10000 cycles. KPFM measurements enable us to successfully explain the origin of the capacitance increase during the cycling study. The strain effect causing the increase

of interlayer spacing was supported by the Raman shift observed in the electrode cycled after 2500 and 10000 cycles. This qualitative study can be applied to other types of transition metal dichalcogenides-based supercapacitor electrodes, which possess a layered nanostructure.

4 Conclusions

WS₂-based electrodes developed via CVD process were tested in a three-electrode cell configuration to explore the mechanisms attributed to the decaying performance of energy storage devices over repeated cycling. Electrodes were extracted at different stages of cycling for analysis of the work function using KPFM. The measurements reveal an increase in capacitance, which is attributed to the strain-induced between the WS₂ layers by ion intercalation/deintercalation during cycling, evidenced by the work function increase and the changes in Raman bands observed with the cycled samples. Thus, the approach provides an ex-situ qualitative analysis capable of monitoring surface properties of the electrodes of direct relation to the performance of energy storage devices.

Conflicts of interest

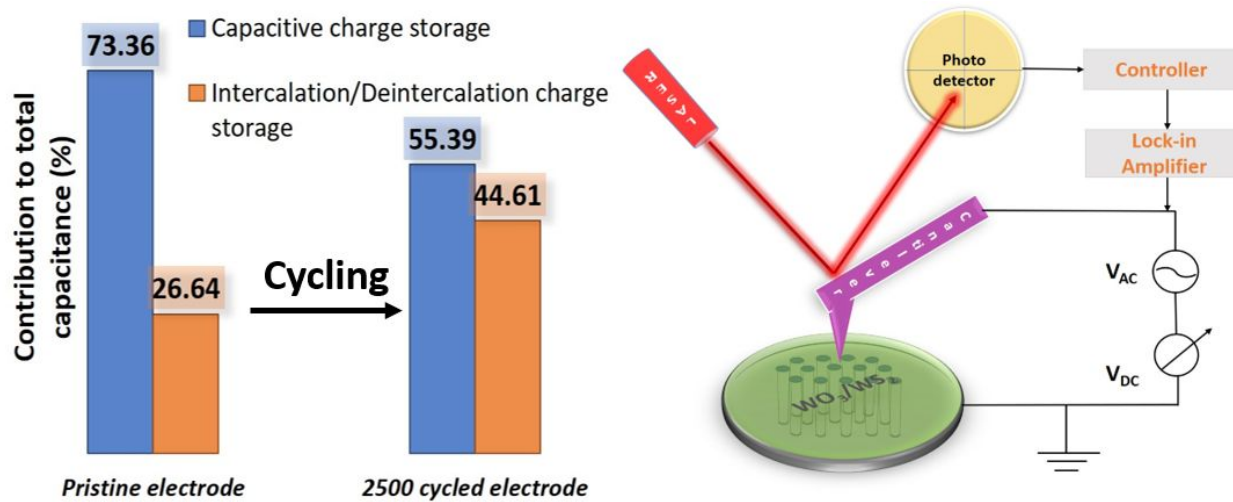
There are no conflicts to declare.

Acknowledgements

J.T. acknowledges National Science Foundation (CAREER: ECCS-1351757 Supplement) for the financial support.

References

1. L. Kouchachvili, W. Yaici and E. Entchev, *J Power Sources*, 2018, **374**, 237-248.
2. S. Chu, Y. Cui and N. Liu, *Nat Mater*, 2017, **16**, 16-22.
3. J. Cherusseri, K. Sambath Kumar, D. Pandey, E. Barrios and J. Thomas, *Small*, 2019, **15**, 1902606.
4. S. Aloqayli, C. K. Ranaweera, Z. Wang, K. Siam, P. K. Kahol, P. Tripathi, O. N. Srivastava, B. K. Gupta, S. R. Mishra, F. Perez, X. Shen and R. K. Gupta, *Energy Storage Mater*, 2017, **8**, 68-76.
5. Y. Y. Tan, D. L. Wu, T. Wang, P. G. Liu, J. Guo and D. Z. Jia, *Appl Surf Sci*, 2018, **455**, 683-695.
6. Q. Cheng, J. Tang, J. Ma, H. Zhang, N. Shinya and L. C. Qin, *Carbon*, 2011, **49**, 2917-2925.
7. F. S. Omar, A. Numan, N. Duraisamy, S. Bashir, K. Ramesh and S. Ramesh, *Rsc Adv*, 2016, **6**, 76298-76306.
8. K. S. Kumar, J. Cherusseri and J. Thomas, *Acs Omega*, 2019, **4**, 4472-4480.
9. W. Melitz, J. Shen, A. C. Kummel and S. Lee, *Surface science reports*, 2011, **66**, 1-27.
10. L. Chen, C. Shi, X. Li, Z. Mi, D. Wang, H. Liu and L. Qiao, *Materials*, 2017, **10**, 273.
11. F. Wang, X. Zhan, Z. Cheng, Z. Wang, Q. Wang, K. Xu, M. Safdar and J. He, *Small*, 2015, **11**, 749-755.
12. Y. Han, Y. Ge, Y. F. Chao, C. Y. Wang and G. G. Wallace, *J Energy Chem*, 2018, **27**, 57-72.
13. K. S. Kumar, N. Choudhary, Y. Jung and J. Thomas, *Acs Energy Lett*, 2018, **3**, 482-495.
14. W. S. Chen, X. Yu, Z. X. Zhao, S. C. Ji and L. G. Feng, *Electrochim Acta*, 2019, **298**, 313-320.
15. X. M. Geng, Y. L. Zhang, Y. Han, J. X. Li, L. Yang, M. Benamara, L. Chen and H. L. Zhu, *Nano Lett*, 2017, **17**, 1825-1832.
16. X. Liu, J.-Z. Zhang, K.-J. Huang and P. Hao, *Chem Eng J*, 2016, **302**, 437-445.
17. S. Ratha and C. S. Rout, *Acs Appl Mater Inter*, 2013, **5**, 11427-11433.
18. N. Choudhary, C. Li, H. S. Chung, J. Moore, J. Thomas and Y. Jung, *Acs Nano*, 2016, **10**, 10726-10735.
19. M. A. Lukowski, A. S. Daniel, C. R. English, F. Meng, A. Forticaux, R. J. Hamers and S. Jin, *Energy Environ Sci*, 2014, **7**, 2608-2613.
20. Z. Z. Cheng, Z. X. Wang, T. A. Shifa, F. M. Wang, X. Y. Zhan, K. Xu, Q. L. Liu and J. He, *Appl Phys Lett*, 2015, **107**.
21. Y. Jung, Y. Zhou and J. J. Cha, *Inorganic Chemistry Frontiers*, 2016, **3**, 452-463.
22. F. Kopnov, Y. Feldman, R. Popovitz-Biro, A. Vilan, H. Cohen, A. Zak and R. Tenne, *Chem Mater*, 2008, **20**, 4099-4105.
23. Y. Yang, H. L. Fei, G. D. Ruan, C. S. Xiang and J. M. Tour, *Adv Mater*, 2014, **26**, 8163-8168.
24. X. He, N. Tang, X. X. Sun, L. Gan, F. Ke, T. Wang, F. J. Xu, X. Q. Wang, X. L. Yang, W. K. Ge and B. Shen, *Appl Phys Lett*, 2015, **106**.
25. L. Meng, Y. H. Zhang, S. Hu, X. F. Wang, C. S. Liu, Y. D. Guo, X. R. Wang and X. H. Yan, *Appl Phys Lett*, 2016, **108**.
26. S. Manzelii, A. Allain, A. Ghadimi and A. Kis, *Nano Lett*, 2015, **15**, 5330-5335.



Novelty of the work

Uncovering the mechanism behind the increase in capacitance of 2D WS₂ supercapacitor electrode upon cycling using KPFM analysis.